Generation of ribbons, helicoids, and complex Scherk surfaces in laser-matter interactions

S. Lugomer* and Y. Fukumoto†

Faculty of Mathematics and Mathematical Research Center for Industrial Technology, Kyushu University, 744 Motooka, Nishi-ku, Fukuoka 819-0395, Japan

(Received 15 July 2009; published 9 March 2010)

Motivated by a diversity of the shape instability phenomena in condensed-matter physics, we study the formation of elastic ribbon structures and transformation into helicoidal structures. Using the multipulse laser-matter interaction with the Co-coated surface, a one-dimensional high-density vortex-filament array has been created. Increasing the number of pulses, the oscillatory strain field causes the cascade of the shape transformations into structures of increasing topological complexity: vortex filaments into ribbons, into ribbon helicoids and tubular-ribbon helicoids, and then into short ribbon structures with the complex Scherk surface being identified. The cascade of transformations follows the scenario in which the topological complexity of the new structure increases with the number of pulses, thus, realizing configurations with more efficient energy relaxation. Above a critical number of pulses, the system is catastrophically disintegrated into small-scale wrinkled and crumpled surfaces. We show that the critical parameter for the ribbon transformations is the number of laser pulses which is equivalent to some critical oscillatory frequency.

DOI: 10.1103/PhysRevE.81.036311 PACS number(s): 47.20.−k, 47.61.−k, 47.80.Jk, 47.32.C−

I. INTRODUCTION

It is well known that nanosecond laser-matter interactions (LMIs) may generate a one-dimensional (1D) array of vortex filaments on a solid surface, with the behavior that is common to stringlike formations of various systems [1–3]. Among them is the action of torsion that generates the Hasimoto solitons [1], formation and instability of vortex rings [4], phenomena such as helicoidal instability, reconnection, and merging of filaments [2], looping of the filaments in the strain field of a point defect, spiraling and pinning [3], etc. All these phenomena are possible due to the fact that vortex filaments (in a certain stage of the LMI) behave as a viscoelastic entity. Their organizational complexity is sensitive on the number of pulses, and various transformation processes into structures of different organizational levels of complexity were observed.

From a more general standpoint of the vortex-filament dynamics and organization, a question arises as to whether the filaments as 1D stringlike formations may transform into two-dimensional (2D) ribbon structures. If so, how does their behavior vary as the number of pulses is increased? The aim of this study is to provide experimental evidence for the transformation of the filamentary into ribbonlike structures on Co-coated steel. The dependence of this transformation on the number of laser pulses is examined.

The melted shear layer of the Co-coated steel behaves, in a certain stage of the nanosecond LMI, like a viscoelastic fluid. Normal stress difference in shearing flows is a fundamental property of viscoelastic fluids [5]. The long ribbons with strongly anisotropic order parameter texture within the vortex sheet are characteristic of the anisotropic fluid mobility and are consistent with driving oscillatory strain field [5,6]. We show, in this paper, that the oscillatory strain field which changes in intensity and topology with the number of pulses causes not a single but a cascade of ribbon transformations. As the number of pulses is increased, filamentary objects go through a succession of transformations of vortex microfilaments into vortex microribbons, into ribbon helicoids, into ribbon-tube helicoids, and then into small-scale structures featured by complex Scherk surfaces, and finally, when the number of pulses reaches the critical value, go through their destruction into wrinkled and crumpled surfaces. Once the number of pulses that generate ribbon-helicoid structures reaches the critical value, the organizational scenario to form a more complex structure is exhausted and the system results in destruction of existing structures, being liable to more efficient energy dissipation.

A distinguishing feature of our experiment is the parametrization of the transformation process in terms of the number of pulses and determination of its critical value. A way of dependence on control parameters, such as the chemical-vapor transport rate, the electric-field frequency, and the mechanical oscillation frequency, is more or less similar to various systems that develop ribbon-type structures. Microribbons and nanoribbons are formed on various materials such as oxides (ZnO) [7–9], SnO_2 [10], biaxial ZnO-Zns [11], ZnS [12], arsenides (GaAs) [13], and selenides (CdSe, ZnSe) [8]. In addition, the semiconductor microribbons and nanoribbons of Si [14], bilayered Si/SiGe [15], oxides of indium [9], gallium [16], titanium [17], $NbSe_3$ [18], as well as of GaN [19] are produced in a number of experiments, in different interaction environments, of using various substrates. The silicon microribbons and nanoribbons, for example, were produced with thickness 80–100 nm, uniform width 3–5 μm, and length up to several centimeters in the patterns of very regular structures or very disordered ones [20]. The similar is true of the carbon nanotube ribbons interpreted as fully collapsed multiwalled carbon nanotubes as observed in TEM micrographs [20–23]. Many of them appear as twisted ribbons of about 28–32 nm width,

*Permanent address: Material Physics Department, Ruder Bošković Institute, Bijenička c.54, 10001 Zagreb, Croatia; stjepan.lugomer@irb.hr

†yasuhide@math.kyushu-u.ac.jp

about 478 (approaching 500 nm) length, and 470 nm periodic distance between twists, with the torsion angle per unit length $\tau=\pi/470$ nm^{-1} [20]. Many of the stripes of various materials appear to be twisted by angles as large as 180°, with the two ends glued to each other, resulting in a one-sided topology as Möbius stripes, as exemplified by the stripes and belts formed on a compound of niobium and selenium $NbSe_3$ obtained by Tanda *et al.* [18]. The belt diameter and width are typically of 100 μm and 1 μm, respectively.

Augmenting the list with recently observed structures, it may be said that the ribbons, ribbon helicoids, double helicoidal structures, as well as the tubular-ribbon helicoids span the range from the atomic scale for physical systems such as superfluid He [6], the nanoscale for biological systems such as peptides [24], DNA molecules [25,26], polymers [27], various spatial scales of ribbons of other materials, extending up the mega- or astrophysical scale in which they take the form of magnetic-flux ribbons [28] and ribbon flares [29] in the stellar atmospheres.

Despite difference of specific features peculiar to the systems, vortex ribbon structures are of fundamental significance with an unequivocal physical interpretation of the organizational complexity classified at a few hierarchical levels that exhibit some common configuration elements.

II. OUTLINE OF EXPERIMENT

Small samples of Co-coated steel of $1\times1\times0.05$ cm have been exposed to the focused beam of a XeCl ultraviolet laser (wavelength $\lambda=308$ nm), of energy $E\sim250-300$ mJ and of the pulse duration $\tau\sim16-20$ ns, in the open configuration, at low repetition frequency of 2 Hz. The smooth surface of Co-coated steel comprised parallel machine-made micron-scale scratches which represent the surface discontinuity. Short Gaussian laser pulses, which illuminate the sample perpendicularly from above, generate a molten surface layer with characteristic gradients of pressure and temperature T. The vertical thermal gradient $\nabla T_{\perp}$ raises the top surface layer which faces the laser beam to the boiling temperature T_b, while the lower surface layer is at the melting temperature T_m. This causes the formation of the shear layer which is accelerated by the Rayleigh-Taylor instability from the center to the periphery of the spot. However, the top layer which has low density and high temperature is moving faster than the bottom one. Any vertical perturbation of the shear layer, like vertical oscillation, causes the formation of the breaking wave. When the Reynolds number (Re) of accelerated fluid reaches the critical value of Re$\sim$103, the Kelvin-Helmholtz (KH) instability sets in, causing transformation of the breaking wave into the roll-up process which generates vortex filaments. In this respect, parallel scratches on the target surface serve exactly to this purpose—to cause vertical oscillation of the accelerated shear layer and the KH instability with formation of micron-scale vortex rolls. In the present experiments, the roll-up process is triggered by the scratches (with the scratch-scratch separation distance $L\sim10$ μm), extending, say, in the x direction on the target surface. Parallel scratch lines cause the transversal perturbation of the shock wave of the form $A\exp(k_p y)$. Here A is the perturbation amplitude equivalent to the height of the scratch wall and k_p is the perturbation wave number: $k_p=2\pi/L$ μm^{-1}. An oscillatory shock perturbs the density interface (shear layer) transversally to the radial flow, or the flow from the central to the peripheral regions (y direction), causing the formation of waves and their roll-up into vortex filaments of the core thickness $\sigma\sim5-7$ μm [1–4]. As a result, a high-density 1D array of vortex filaments (the separation distance between neighboring filaments $\Lambda\leq\sigma$) has been generated.

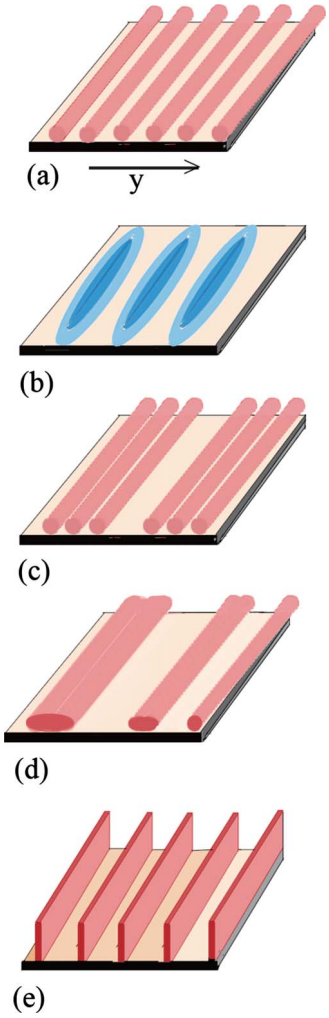

FIG. 1. (Color online) Schematic view of transformation of a 1D vortex-filament array into a 1D ribbon array. (a) A 1D vortex-filament array. (b) Oscillatory perturbation generates the stationary wave of the strain field. Dark blue regions designate the region of strong strain field. (c) Grouping of vortex filaments in the regions of weak strain field. (d) Merging of vortex filaments due to lateral compression. (e) A 1D ribbon array.

The multipulse laser irradiation induces oscillatory strain imposed on the vortex-filament array generating strong lateral compression. Increasing the number of pulses, the strain field becomes inhomogeneous causing transformation of vortex filaments into more complex structures (Fig. 1). The structures are quenched and stay frozen permanently due to ultrafast cooling after pulse termination, thus, making possible *a posteriori* analysis of their micrographs.

The frozen surface structures have been studied in the reflective mode of the Nikon optical microscope and registered by a CCD camera. The best pictures of the surface structures were obtained by tilting the table of the microscope. Only a slight tilting is needed to get the view angle with the depth of the observed object(s). If the tilting angle is too large, the objects become dark and actually cannot be observed. The optimization of the view angle was performed for every new sample or analyzed spot by repeated adjustment of tilting. Further optimization of the picture is obtained by the variation in color which illuminates the sample (by the change in the optical filters), as well as by the variation in the illumination intensity.

III. RESULTS AND DISCUSSION

A. Transformation of vortex filaments into ribbons

Once the filaments are formed after the first few pulses [Fig. 1(a)], the subsequent pulses in a train cause the formation of a strain-wave field oscillation with constant phase [Fig. 1(b)], which brings about almost coherent perturbation, with little modulation, of the filament array. Exposed to the oscillatory strain field, the filaments come close to each other, becoming grouped in the regions with the minimal strain [Fig. 1(c)]. The lateral compression caused by the oscillatory strain induces their axial merging into ribbons [Fig. 1(d)]. The longer axes of flattened filaments are parallel to the surface and lie inside the shear layer. The stationary strain wave field drives the ribbons, formed by $N>10$ pulses, so as to be positioned in the regions of minimal compression (between two maxima), thus, generating almost a regular array of ribbons with their surface perpendicular to the substrate, as schematically shown in Fig. 1(e).

The laser generation of ribbons and their perpendicular orientation to the target surface depend on a number of parameters such as the surface and the laser beam characteristics as well as the spot size. Their formation is very sensitive on the characteristics of the surface discontinuity (scratching periodicity and amplitude) as the initial topological condition for the generation of instability. If the sample surface is identically scratched in all experiments, and the surface periodicity is comparable to the filament core size $\Lambda \sim \sigma$, the vortex filaments merge into ribbons under a series of pulses. Variation in the scratch periodicity, scratch amplitude, etc. causes different organization of the filaments and does not lead to formation of ribbons. If the laser power which generates the vertical-strain component is adequate, the ribbons get turned into a vertical position and move into the regions of low oscillatory strain. If the power is too small, the ribbons stay in the position parallel to the surface. Finally, the spot size should not be too small, say, of the micron scale, because too small spot represents the confined space for the oscillatory strain field evolution, for the filament formation, as well as for their self-organization into ribbon structures.

When the ribbons are formed and organized into the vertical position, their conformations are affected by the number of pulses. By increasing the number of pulses, the oscillatory strain field becomes irregular and the ribbon organization becomes complex and disordered. A typical example of an

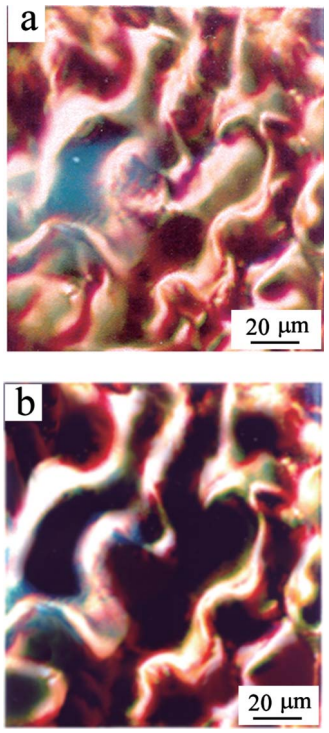

FIG. 2. (Color online) Pattern of the ribbon structures. (a) Optical micrograph of the long and short ribbon structures formed after $N=17$ pulses. (b) Optical micrograph after numerical filtration and removal of the short structures of (a). The long parallel deformed ribbons are clearly seen.

almost disordered ribbon array formed after $N=17$ pulses is shown in Fig. 2(a). A microscopic analysis reveals an arrangement of long ribbons separated by an empty space, in which the other type of smaller structures is observed. Thus, the pattern indicates two types of underlying dynamics: the primary dynamics which forms the ribbons and the secondary short curved filaments bridging the parallel ribbons. The numerical filtration and elimination of the smaller structures manifests that ribbons of length $L \sim 80-150$ μm, as the primary structures, are organized into a 1D array with (average) periodicity $\Lambda \sim 25-30$ μm [Fig. 2(b)]. The ribbon width takes $W \sim 15-22$ μm, and thus their aspect ratio $A=L/W$ ranges from $A \sim 4$ to 10. The refined micrograph in Fig. 2(b) discloses undulation of the ribbons with wavelength $\lambda \sim 15-30$ μm deformed by development of kinks, dips, and short local helical configurations.

The configuration observed in the micrograph Fig. 3(a) (i) clearly shows that merging of the filaments into a ribbon occurs along their whole length, except at the bended segments whose cores are separated for $\Lambda \sim 20-25$ μm, i.e., for the distance $\Lambda \gg \sigma$, as schematically shown in Fig. 3(a) (ii). The micrographs in Fig. 3(b) visualize the development of (i) large undulation, (ii) dip, (iii) kink, and (iv,v) loop which are all traced to twisting and writhing of the ribbons. This indicates that, at $N=17$, the inhomogeneous oscillatory strain field already evolves into the micron-scale twisting and writhing domains (strain field point defects), which switches on various types of perturbations of the ribbons.

A description of the observed ribbon configurations can be made in the language of its topological ingredients such

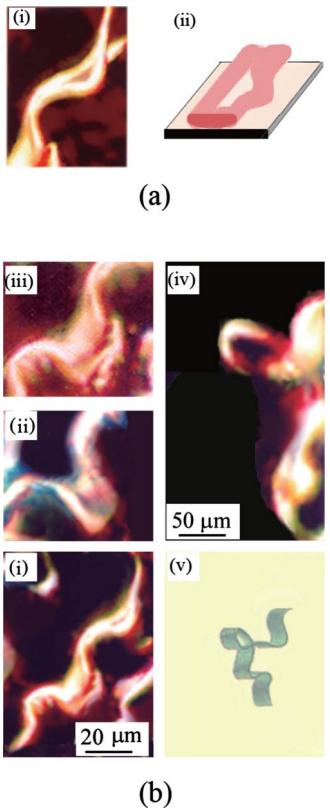

FIG. 3. (Color online) Detail of the ribbon formation by merging of filaments. (a) Vortex filaments merge into ribbons at all places where the filament-filament distance $\Lambda \leq \sigma$ merging does not occur at bended filament segments where $\Lambda > \sigma$. (b) Optical micrograph showing configuration of the ribbon segments: (i) undulation, (ii) dip, (iii) kink, (iv) loop, and (v) schematic ribbon-loop reconstruction.

as the writhe and the twist whose summation is invariant during an inviscid motion [30], though ribbon structure may become involved in time. Define the centerline along the ribbon tube C by $\boldsymbol{X}=\boldsymbol{X}(s)$, parametrized by the arclength s along $\boldsymbol{X}$. We attach, to each point on $\boldsymbol{X}(s)$, a segment $\boldsymbol{N}(s)$ of length ϵ, lying on the ribbon surface, normal to the tangent vector to C. We may call the collection of $\boldsymbol{N}(s)$ the director field. Suppose that $\boldsymbol{N}(s)$ is based at $\boldsymbol{X}(s)$. The collection of the end points $\boldsymbol{X}^*(s)$ of $\boldsymbol{N}(s)$ constitute a curve and the linking number L_k of the two curves $\boldsymbol{X}$ and $\boldsymbol{X}^*$, with distance ϵ to each other, serves as a topological invariant of the ribbon. We calculate the twisting angle of the spanwise director field $\boldsymbol{N}$ along $\boldsymbol{X}$. Let $\boldsymbol{t}=d\boldsymbol{X}/ds$ be the unit tangent vector along C, $\boldsymbol{n}$ be the unit principal normal, and $\boldsymbol{b}=\boldsymbol{t}\times\boldsymbol{n}$ be the unit binormal vectors. Let $\theta(s)$ be the angle of the spanwise vector relative to $\boldsymbol{n}$. Then $\boldsymbol{N}(s)$ is expressed as

$$\boldsymbol{N}(s) = \epsilon \cos\theta \boldsymbol{n}(s) + \epsilon \sin\theta \boldsymbol{b}(s). \tag{1}$$

In order to have an idea of the twist, we revisit the example a ribbon surface θ=const [Fig. 4(a)] [31]. The ribbon boundary consists of the curve C and the curve Γ_θ of θ =const, with distance ϵ to each other. Let L_k be the Gaussian linking number of (C,Γ_θ). We now introduce a new angle variable,

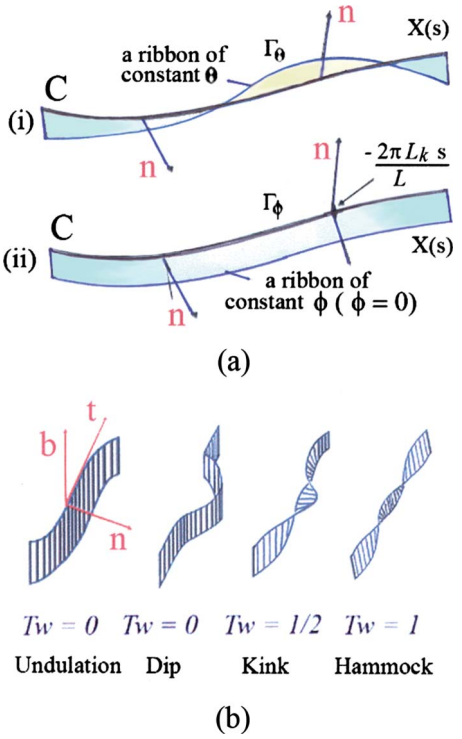

FIG. 4. (Color online) Illustration of the ribbon topology. (a) (i) Ribbon θ=const with boundaries C and Γ_θ which have linking number L_k; (ii) ribbon ϕ=const with boundaries C and Γ_ϕ which have zero linking number (courtesy of The Royal Society, Fig. 2 (a drawing) from the journal: Proc. Royal Society A, by Chui and Moffatt, from the paper "The Energy and Helicity of Knotted Magnetic Flux Tubes," Ref. [31]). (b) Schematic presentation of the ribbon shape instability: undulation, dip, kink, and hammock, with the corresponding values of twist T_w, from left to right.

$$\phi = \theta + 2\pi L_k s/L, \tag{2}$$

where L is the total length of C. This choice is called the zero framing and has the property that the ribbon of ϕ=const is *untwisted* in the sense that its boundary curves (C,Γ_ϕ) have zero linking number.

We are now prepared to introduce, for a general ribbon, the total twist T_w, the writhe W_r, and their relation to the linking number L_k [30]. The total twist number of the ribbon is defined by

$$T_w = \frac{1}{2\pi}\oint_C \left(\boldsymbol{N}\times\frac{d\boldsymbol{N}}{ds}\right)\cdot\boldsymbol{t}ds = \frac{1}{2\pi}\oint_C \left(\tau + \frac{d\theta}{ds}\right)ds. \tag{3}$$

The total twist T_w is the sum of the normalized integral of torsion τ of the curve C and of the variation $d\theta/ds$ of the angle relative to $\boldsymbol{n}$. The writhe W_r is defined by

$$W_r = \frac{1}{4\pi}\oint_C \oint_C \frac{(\boldsymbol{X}-\boldsymbol{X}')\cdot(d\boldsymbol{X}\times d\boldsymbol{X}')}{|\boldsymbol{X}-\boldsymbol{X}'|^3}. \tag{4}$$

The Călugăreanu theorem states that the Gauss linking number L_k of $\boldsymbol{X}(s)$ and $\boldsymbol{X}^*(s)$, a topological invariant, comprises two parts, the writhe and the twist contribution:

$$L_k = T_w + W_r. \tag{5}$$

The helicity $\mathcal{H}$ is a topological invariant of the continuum; it does not change under continuous deformations. It is tied with the linking number via $\mathcal{H}=\Gamma^2 L_k$, where Γ is the circulation of a bundle of vortex filaments constituting the ribbon [30]. The writhe and the twist, if taken separately, are not topological invariants and their values of T_w and W_r change according to the change in geometry, implying the occurrence of interchange between T_w and W_r during continuous deformation [32].

The writhe W_r is characterized by the following properties: (i) W_r depends only on the geometry of the ribbon-tube axis C; (ii) W_r is invariant under rigid motions or dilations of the space containing C but its sign is changed by reflection. The total twist T_w has the following properties: (i) T_w is a continuous function of C (even through self-intersection); (ii) T_w is invariant under rigid motions or dilations of the space containing the tube, but its sign is changed by reflection, T_w is additive. The total torsion T_w is partitioned into the total torsion and the *intrinsic twist* as displayed in the form of Eq. (3). The total twist is a continuous function of C, but the total torsion and the intrinsic twist may be discontinuous in deformations of the tube axis through an inflection point, a point of vanishing curvature [30]. At an inflectional configuration, the twist is abruptly converted into the writhe or vice versa. This abrupt conversion of the twist into the writhe could be the origin for the kink instability [32,33].

Suppose that an open ribbon is thought of as a large half segment of a ribbon loop, whose initial helicity is zero [32]. A vortical and shearing boundary motions generate some twisting motions of the ribbon-tube structure of vortices, increasing the twist. This process continues until the critical value for the internal twisting of the field lines is reached, the threshold being determined by the geometry of the ribbon tube and tension [32,33]. When the growth of internal twist is no longer tolerated, a further increase in the twist by boundary motions may be converted into the writhe until a force-free equilibrium is reached and, correspondingly, a dip is formed. In a later stage, a further writhing of the flux tube is also impeded and a kink mode instability emerges. In forming a hammock configuration, the vortex ribbon-tube centerline must pass through an inflectional configuration accompanied by a change in concavity. The conversion of the twist into the writhe is well captured by the following local representation of the ribbon-tube axis $\boldsymbol{X}=(x,y,z)$:

$$x = a\cos\xi - cT_w\cos 2\xi, \quad \xi \in [-\pi/2, \pi/2],$$

$$y = b\sin\xi - cT_w\sin 2\xi, \quad T_w \in [0,1],$$

$$z = cT_w\sin\xi, \tag{6}$$

where a, b, and c are configuration parameters; ξ is a polar angle [32,33]. The schematic three-dimensional presentation of the ribbon undulation, dip, kink, and hammock configurations for $T_w=0, 1/2, 1$ are shown in Fig. 4(b). It is likely that the instability converting the twist to the writhe is associated with transition to a lower energy state.

Identification of the experimental parameters for the formation of ribbons is, though of importance, limited to be at a qualitative level. We found that formation of ribbons does not occur at the low density vortex-filament array ($\Lambda \gg \sigma$), but only at the high-density one ($\Lambda \leq \sigma$). It means that there exists a critical filament-filament separation distance Λ_c, the corresponding critical wave number k_c, and the critical frequency Ω_c of the oscillatory strain field, which enable the formation of ribbons. When these critical parameters are attained, the lateral compression causes the confinement of filaments moving them into the vertical position (one over the other) and then merging them into ribbons [Fig. 1(e)]. Namely, compression of the shear layer generates the strain field which is strong in the vertical direction. The strain field requisite for the ribbon formation is the normal strain component developed at the critical oscillatory frequency.

The organization of ribbons into a 1D array is the process that creates the empty space between the ribbons, a kind of a wall defect. In this empty space, the oscillatory excitation causes creation of the new vorticity and the evolution of smaller structures. These secondary structures are separated from the ribbons but may eventually merge with the remnants of the filaments which were not annihilated. They reveal characteristics different from the ribbons, as a result of different local dynamics of the shear layer in the empty space between the ribbons.

The above process of 1D ribbon array formation in multipulse LMI is the characteristic of a more general scenario in which vortex filaments experiencing the oscillatory compression, whereby vortex filaments are arranged to form vertical vortex sheets. Becker and Shelly [5] found that an elastic filament embedded in a shear flow yields a normal-stress difference, which is especially large for the oscillating shear. As a consequence, the filament may move not only horizontally but also vertically, out of plane, and change its shape. A local curvilinear flow may exert a driving force of non-Newtonian property like climbing up at the critical shear rate. The origin of such filament behavior lies in the elastic instabilities on the microscopic scale occurring when the compressional stresses are sufficiently large as to create large normal-stress differences [5,6]. A similar effect was observed for the ^{3}He-A superfluid in which the filaments are collected to form vortex stripes and sheets [6]. The formation of stripes, induced by the system rotation, takes place when the rotational frequency reaches the critical frequency. The analogy between the phenomena in LMI and in the superfluid ^{3}He leads us to the speculation that the transition from the filamentary to the ribbon structures is determined by the relaxation rate toward the instantaneous equilibrium. First, the order-parameter texture becomes locally unstable around a nucleation center and the creation of a domain-wall defect follows. When the rotation speed is increased, the new vorticity reenters in this planar defect, whereby the critical velocity is reduced and the mobility is enhanced. Eltsov *et al.* [6] observed that, in a rapidly oscillating drive, a single sheet becomes unstable and transforms into multiple sheets.

B. Transformation of vortex ribbons into ribbon helicoids

Increasing the number of pulses to $N=17-20$ causes transformation of a 1D ribbon array into an inhomogeneous

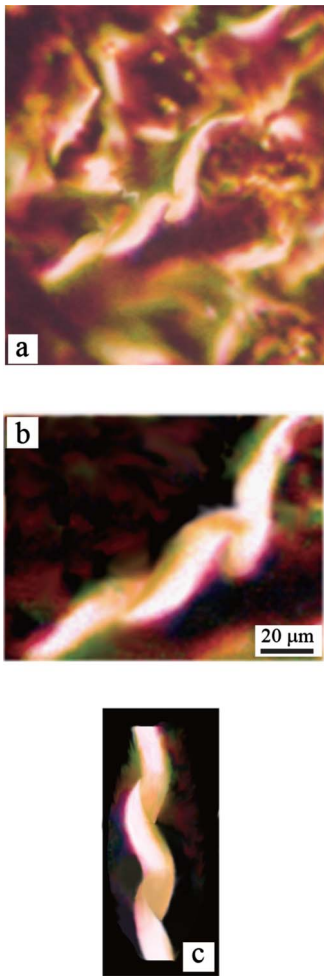

FIG. 5. (Color online) Increasing the number of pulses to $17 < N \leq 20$ causes the shape instability of ribbons. (a) Optical micrograph showing the transformation of the pattern of parallel ribbons into the inhomogeneous pattern of more complex ribbon structures. (b) Micrograph of typical structure extracted from the pattern in (a), by numerical filtration and reconstruction, reveals a screw surface with pitch about 60 μm. (c) Reconstruction of the screw structure in (b).

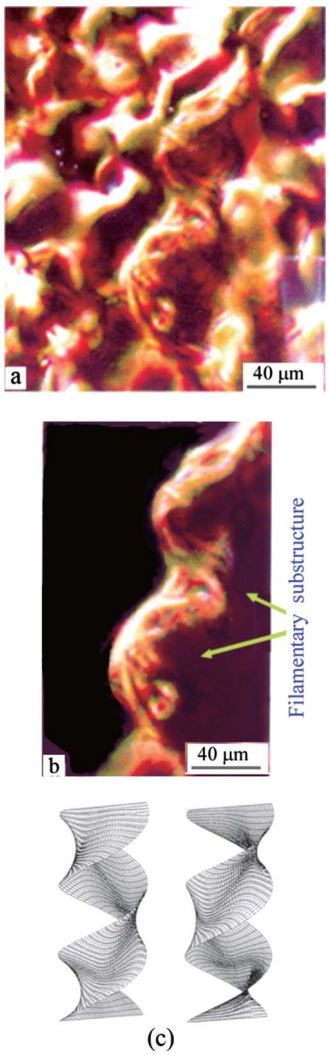

FIG. 6. (Color online) Complex pattern of ribbon-type structures after the shape transformation. (a) Optical micrograph showing the pattern of ribbon-helicoid structures formed at $N=18$ pulses. (b) Ribbon-helicoid structure extracted from (a) by numerical filtration. Notice that the ribbon width is increased compared with Fig. 2, the starting one. The refined picture makes visible substructures of the ribbon helicoid made up from a collection of individual filaments which are not completely merged. (c) Two ribbon-helicoid surfaces obtained by numerical simulation for the aspect ratio $h/W=2$ and a winding number $\phi_0/\pi=3$ (copyright Am. Phys. Society: courtesy of Boudaoud, from Ref. [34]).

pattern of more complex ribbon structures as shown by Fig. 5(a). A numerical filtration and reconstruction of typical structure extracted from the pattern in Fig. 5(a) manifests the screw surface with pitch about 60 μm [Figs. 5(b) and 5(c)]. Another pattern of complex ribbon structures is shown in Fig. 6(a). The most informative structure extracted from the pattern after filtration is displayed in Fig. 6(b). This structure favorably compares with a helicoid, or more precisely with the intermediate structure between a ribbon and a ribbon helicoid, formed as a consequence of the shape instability. Such an instability occurs when the growing number of pulses induce an oscillatory strain field that executes a strong twisting action on the ribbons. The nonhomogeneous twisting action transforms the ribbons into various kinds of helicoids. In addition, the ribbons undergo writhing which causes a number of effects including change in the aspect ratio and formation of kinks. The aspect ratio of a helicoid is defined by $A=h/W$ where W is the length of the rule constituting the surface and h is the pitch of the helicoid [34].

The classical continuum theory for chiral ribbons by Helfrich and Prost [35] rests on the assumption that the ribbon is *isometric* signifying that it does not support elastic strain [36]. Chiral twist can be imposed on isometric, or nonstretchable, ribbons only by winding them around the surface of a cylinder or a cone, being consistent with the observed spiral ribbon and tube or a set of tubular (rope) structures [36,37]. On the other hand, if one does allow a ribbon to be stretched but forbids any lateral bending along its axis, then the geometry of the ribbon is restricted to a family of *ruled surfaces*, that is, surfaces generated by the motion of a line

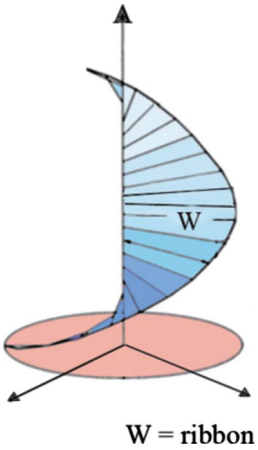

FIG. 7. (Color online) Illustration of the helicoid as a ruled surface formed by the circular motion of a rule.

[38]. This family includes the helicoid, a twisted minimal surface [Fig. 6(c)] [38–40].

The shape instability which transforms a ribbon into a ribbon helicoid can be described by a physical model which takes account of finite thickness, elasticity, and stiffness. The most appropriate model is the one of Boudaoud *et al.* [34] which describes the formation of a helicoid from the soap film and its instability. For a forced harmonic excitation, the vibration equation of a minimal surface is reduced to the time-independent 2D Schrödinger equation. An attractive potential of modified Pöschl-Teller type corresponds to the helicoid, which admits the eigenfunction to be written in terms of the hypergeometric functions. The construction of a helicoid is shown in Fig. 7. A helicoid under question has height $h=A\phi_0$ and the diameter $W=2A$ sinh θ_0, being both fixed, where A is some length parameter. The marginal stability of the helicoid is attained at a critical value of θ_0 ($\theta_0>1.195$) depending on the aspect ratio h/W. When the twist angle ϕ_0 is increased, an instability is switched on, causing destruction of the helicoid and generating a ribbon surface which lies on helices [34].

A close examination of Fig. 6(b) indicates that this structure is not exactly a helicoid, but some transitional (intermediate) structure between the isometric (not elastic) ribbon and the (elastic) helicoid, a continuous transition [34]. The ribbon-helicoid structure in Fig. 6(b) closely resembles the numerically simulated chiral ribbons of Seliger *et al.* [41], who found that they can be obtained by a smooth interpolation between the helicoid and the isometric spiral ribbon with no discernible transition point. This result was obtained by a Monte Carlo simulation of their lattice model for which the ribbon elasticity is characterized by three elastic parameters: K_{bending}, $K_{\text{stretching}}$, and K_{twist} (or the chiral elastic constant) with $6\leq K_{\text{stretching}}\leq 10$. Accordingly, the ribbon-helicoid structures formed in the multipulse LMI possess significant elasticity which makes possible the formation of surfaces more complex than the ruled surfaces. However, the ribbon elasticity is smaller than that of a single filament. Intuitively, a narrow ribbon is more elastic than a wide one [41].

The measurement of the width, the thickness, and the length of the ribbons as functions of the number of pulses

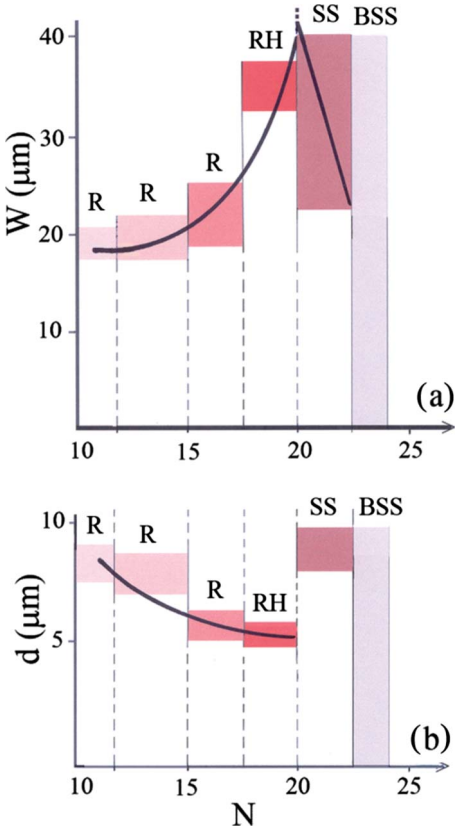

FIG. 8. (Color online) Variation in the ribbon elasticity as a function of the number N of pulses. (a) Diagram showing the nonlinear increase in the ribbon width W with N. The ribbon width gradually grows above $N=13$, grows faster for $15\leq N<17$ and, for $N\geq 17$, drastically increases to the maximum value of $W\geq 40$ μm, where the breakup of the long ribbon structures into Scherk-surface structures occurs. The breaking of the long ribbons into short structures leads to decrease in W. (b) Diagram showing the corresponding nonlinear decay of the ribbon thickness d with N, up to the transition point into the Scherk-surface structures where the ribbon thickness drastically increases (legend: R—ribbon; RH—ribbon helicoid; SS—Scherk-surface structures; BSS—breakdown of the Scherk-surface structures).

has shown somewhat different characteristics. The ribbon width increases in a nonlinear way, from $W\sim 18-20$ μm for $N=17$, to $W\sim 30-35$ μm for $N=20$, up to almost $W\sim 40$ μm for $N=23$ [Fig. 8(a)]. The initial ribbon thickness of $d\gtrsim 7$ μm is comparable or slightly larger than the core size of the parent vortex filaments. This effect is caused by the axial merging in which the filament circulation changes into the ribbon circulation. In this process, the circulation strength of the ribbon is slightly reduced with respect to that of the filament one causing the ribbon thickness to be slightly larger than the filament core size. As the number of pulses increases, the initial ribbon thickness correspondingly decreases from $d\gtrsim 7$ μm for $N=13$, to about 5 μm for $N=17$, and finally below 5 μm [Fig. 8(b)]. This may indicate an opposite behavior from that mentioned by Seliger *et al.* [41]; the elasticity increases with increasing of the width. Another reason for such behavior is inferred from the fact that the micrograph reveals five vortex filaments in the rib-

bon structure which are not completely merged [Fig. 6(b)]. The increase in the ribbon elasticity in this case originates dominantly from the increase in the gap between neighboring filaments with increasing N.

The helicoids as minimal surfaces are of common occurrence in many soft matter systems ranging from helicoidal organization of lyotropic and thermotropic liquid crystals [42], helicoidal macromolecules, to transformation to ribbons of A-DNA and P-DNA [34]. Examples of intermediate cases between ribbons and helicoids comprising certain elasticity called chiral ribbons are available in biological systems [43].

C. Transformation of vortex ribbons into ribbon-tubular-helicoidal structures

The other type of the ribbon transformation generated at $N=17-20$ is the ribbon-tubular-helicoidal structure as shown in Fig. 9(a) with its numerically filtered object Fig. 9(b). This structure could be formed if the ribbon is deformed in such a way that two of its ends start approaching motion rolling around the central axis and are glued together, constituting a tubular surface of circular cross section [Fig. 9(c)]. In the next step, the tube is twisted around the cylinder [44]. Such tubular structures can only be formed when the width W of the ribbon, increasing with the number of pulses, reaches some minimal value necessary for completing the rolling-up motion. The estimation of W from the micrograph [Figs. 9(a) and 9(b)] indicates as wide as 40 μm. Such a transformation requires that the elasticity, the bending, and the torsional stiffness of the ribbon preserve their integrity. From the mathematical viewpoint, a circular screw surface can be generated by moving a circle under a continuous screw motion. The shape of the surface depends on the orientation of the generating circle. The three types of such surfaces numerically constructed by Havlicek [44] are reproduced in Fig. 9(d). On the right-hand side (iii), the plane of the circle which makes a helical motion is *horizontal* (orthogonal to the *vertical* axis of the screw). Typical structures of this type were obtained on carbon microcoils by metal catalyzed pyrolisis of acetylene as it can be seen in Fig. 6(b) of Motojima and Chen [21]. In the middle (ii), the plane of the circle is *vertical*. The surface (i) is a screw pipe surface which is the envelope of a sphere subject to a continuous screw motion. In this case the generating circle is neither vertical nor horizontal. Although, at first glance, these surfaces may look alike, their geometric properties are quite different [44]. The third structure may be identified with the coiling of a filamentary rope around the cylinder and seems to bear resemblance with the structure in Figs. 9(a) and 9(b). We remark that this structure is also similar to the magnetic filament rope of Zeldovich *et al.* [45] in dynamo process.

The ribbon-tubular-helicoidal structure [Figs. 9(a) and 9(b)] as well as the ribbon-helicoid structure [Fig. 6(b)] disclose the existence of fine substructures of a bundle of vortex filaments. It is clearly seen that several vortex filaments, though not being completely merged, are twisted in a collective way.

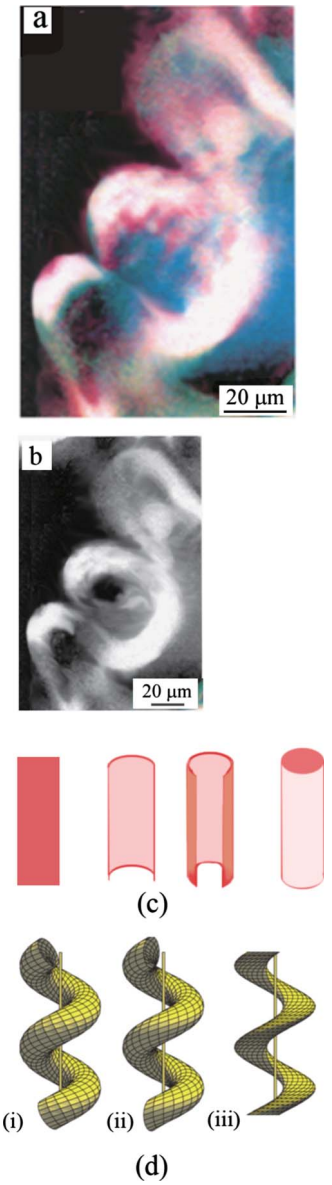

FIG. 9. (Color online) The transformation of a ribbon into a ribbon-tubular helicoid generated at $17<N\leq 20$. This type of structure appears if the ribbon is deformed in such a way that it rolls up around the central axis to form a circular cylindrical surface with the two ends glued together. Thereafter, the tube is twisted around the cylinder. (a) Optical micrograph of a ribbon-tubular helicoid. (b) Numerically filtered micrograph from (a). (c) Process of the tubular-ribbon-helicoid formation for forming a ribbon tube of circular cross section (from left to right). (d) In the next step, the ribbon tube is twisted around the cylinder giving rise to the tubular-ribbon helicoid, with the following characteristics. (i) The surface is a screw pipe surface which is the envelope of a sphere subject to a continuous screw motion; (ii) the plane of the generating circle is vertical; (iii) the circle is horizontal (courtesy of Havlicek of T.U. Vienna; from Ref. [44]).

D. Breakdown of vortex ribbon helicoids and ribbon-tubular helicoids: Complex Scherk-surface structures

Increasing the number of pulses to $N=20-23$ causes breakdown of the ribbon helicoids and ribbon-tubular heli-

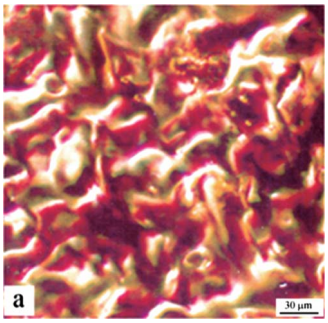

FIG. 10. (Color online) Optical micrograph showing a very complex pattern of the small-scale ribbon structures of the Scherk-surface type, formed by the breakdown of the long ribbon-helicoid and tubular-ribbon-helicoid structures, above $N=23$.

coids into small-scale structures (Fig. 10). The image filtration and analysis reveal only small fragmented segments with a wavylike surface, the surface with curled edges, etc. Such catastrophic transformation occurs if the deformation of helicoids and companion tubular structures surpasses their elasticity limit. The growth of strain causes mechanical instabilities of elastic surfaces over a wide range of scales depending on N as the critical parameter. Typical small-scale structures selected from the complex pattern resemble the complex Scherk surfaces with characteristic edge curling [Fig. 11(a)]. A comparison of these surface structures with numerically generated complex Scherk surfaces in Fig. 11(b) [40] exhibits a close similarity. In contrast to a helicoid which has minimal Scherk surface, these structures have the mean curvature $H \neq 0$ [39].

The increase of N to $N > N_{cr}(=23)$ causes breakdown of the small Scherk-surface structures, generating even smaller structures of larger curvature with buckling which become merged into crumpled surfaces. The irregular oscillatory shocks increase the deformation of a surface generating new wrinkles and ridges. The crumpling of an elastic sheet appears to be a highly effective channel for the energy relaxation. As crumpling proceeds with increasing N, the deformation energy tends to concentrate in narrow ridges so that a vicious flow between the structures is induced.

Similar small-scale structures which show buckling were found in the pattern of compressed membranes connected with buckling dynamics [46,47]. Membranes develop wavy patterns whose wavelength grows via coarsening, similarly to rough growing surfaces. The analogy extends even to polymerized membranes formed from equilibrium buckling dynamics of thin elastic sheets in a viscous medium [46]. Furthermore, an analogy is drawn with phenomena of the astrophysical scale as exemplified by the magnetic-field ribbons and ribbon-tubular structures evolving from the magnetic-flux filaments. The magnetic ribbons, helicoids, and tubular structures grown by merging close filaments and then exposed to twisting and writhing were studied in connection with the astrophysical dynamo [48,49]. The electric filament and ribbon structures were generated in a magnetic field driven by the ac electric field. The transition between the structures was induced by variation in the electric-field frequency [49]. The oscillatory electric field plays, in the

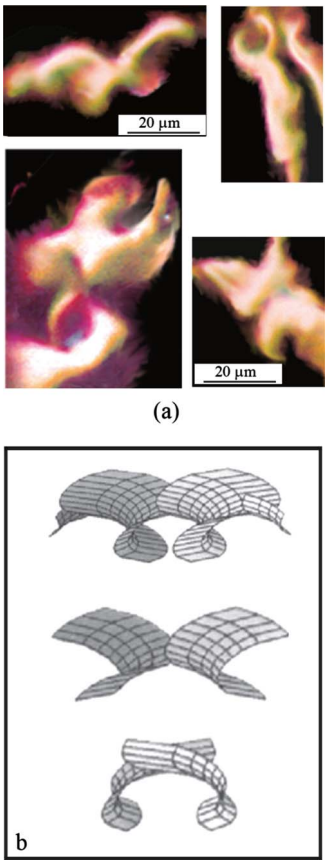

FIG. 11. (Color online) The small-scale Scherk-surface structures. (a) Typical structures extracted from Fig. 10 manifest the characteristics of the complex Scherk surface. (b) The complex Scherk-surface structures obtained by numerical simulation [courtesy of Console and Fino from Lecture Note "Geometria Riemaniana delle Superfici" [40], Capitolo 12, "Le Superfici Minimali" (http://www.dm.unito.it/personalpages/console/Dispense/superfici.pdf)].

LMI, the role of the oscillatory strain field generated by the series of pulses. Cattaneo's electrochemical experiment of using oscillating electric field [48] simulates the astrophysical dynamo formation by a multiple parallel arrangement of individual electric-flux filaments, which is responsible for the current amplification [49]. At a critical frequency, the electric ribbons become broken into short deformed segments that resemble the crumpled membrane with fractal surface characteristics.

E. Nonlinear pattern selection and limits of self-organization

The multipulse LMI generates structures which are born in the form of vortex filaments and transform into progressively complex structures with increasing the number N of pulses. Starting with the filaments at small N, the ribbons appear in the range $N=10-17$. The increase of N from 17 to 20 causes the transformation of ribbons into helicoids and ribbon-tubular structures. These shape transformations represent the switch of the system from an energy relaxational channel into a more efficient one, establishing gradually increasing level of the organizational complexity (Fig. 12). Reaching the ribbon-helicoid and ribbon-tubular state, the

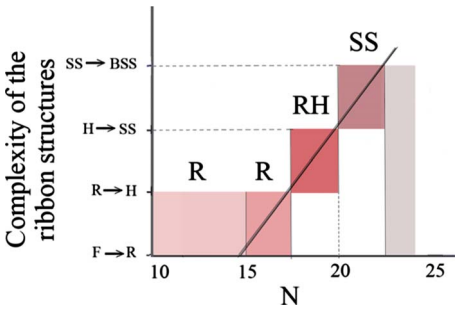

FIG. 12. (Color online) Qualitative diagram showing the complexity of the ribbon structures as a function of N. The complexity increases with N up to $N \geq 23$, when the breakup of the Scherk-surface structures into wrinkled and crumpled structures occurs [legend: F R (filament into ribbon transition); R H (ribbon into ribbon-helicoid transition); H SS (helicoid into Scherk-surface structure transition); SS BSS (breakdown of the Scherk-surface structures)].

system has attained the high level of the organizational complexity. When the number of pulses exceeds $N=20$, the system cannot develop a more complex pattern organization based on the long ribbons, helicoids, and tubes; the elongated structures are disintegrated into short ribbon structures endowed with characteristics of the complex Scherk surfaces. These surfaces represent the limit of self-organizational complexity. Further increase of N beyond $N=23$ causes a violent breakdown of the short ribbon Scherk-surface structures into wrinkled and crumpled surfaces, as the most efficient instantaneous relaxational channel.

IV. CONCLUSION

The multipulse laser-matter interaction on the Co-coated steel target surface, endowed with parallel scratches, in the open configuration generates a 1D high-density array of vortex filaments with the periodicity $\Lambda \leq \sigma$. As the number N of pulses is increased, the oscillatory strain field developed in the stationary wave field causes the filament grouping and merging into ribbons due to lateral compression. The normal strain component (which is always present under compression) causes the vertical organization of the ribbons with respect to the target surface, and formation of a 1D ribbon array. Further increase of N causes strong perturbation of the array, generating undulations, kinks twists, dips, and other ribbon configurations. At the same time, in the flat fluid space between the ribbons (which in the topological sense represents the quasi-2D wall defect), secondary vortices are created, leading to development of the short-scale structures. The observed ribbon configurations are well described on the basis of their topological properties such as the total twist, the writhe, and the linking number [30,33].

The increasing number of pulses causes gradual transformation of vortex ribbons into structures with increasing level of complexity. Two of such structures are identified: ribbon helicoids and ribbon-tube helicoids. Due to the fact that ribbons have width, thickness, elasticity, and stiffness, the new structures are rather the intermediate ones between ribbons and ribbon helicoids. Such real (physical) structures are well described in a framework developed by Boudaoud *et al.* [34]. Their model describes such structures on the basis of a solution of the time-independent Schrödinger equation with an attractive potential wall of so-called "modified Pöschl-Teller" type. Simultaneously with the ribbon helicoids, the other structures such as tubular-ribbon helicoids are observed. According to Havlicek [44], these structures are formed if the ribbon is deformed in such a way that two of its ends start approaching motion around the central axis and meet together to form a cylindrical surface of circular cross section. As the next step, the tube is twisted around the cylinder. The tubular structures can be formed when the width W of the ribbon exceeds some critical value which makes possible approaching circular motion of both ends of the ribbon. Our estimation is $W > 40$ μm for occurrence of this rolling-up process of the ribbon. Such transformation requires that the elasticity, bending, and stiffness of the ribbon preserve its integrity. As a geometric construction, a circular screw surface can be generated by moving a horizontal circle with a continuous screw motion [44].

Continuing the increase of N causes breakdown of ribbon helicoids and tubular-ribbon helicoids into short structures. Namely, the enhanced strain causes mechanical instabilities of elastic surfaces. Typical small-scale structures selected from the complex pattern resemble the complex Scherk surfaces with characteristic edge curling. Further increase of N causes, if N goes beyond a certain value, breakdown of the complex Scherk-surface structures, generating even smaller structures with buckling, which are merged into crumpled surfaces. The irregular oscillatory shocks increase the deformation of a surface generating new wrinkles and ridges. Crumpling of an elastic sheet provides a highly effective means for the energy relaxation.

Our analysis of complex patterns of ribbon structures on the Co-coated steel strongly indicates that, under oscillatory strain field, the organization of structures changes with increasing N, becoming more complex. This process is caused by the tendency of the system to select a configuration suited to more efficient energy relaxation. The process of upgrading organizational complexity with increasing N does not continue indefinitely owing to some constraints posed by the material integrity. At a critical value of N, the organizational process turns into disintegration of the complex surface structures, thus, catastrophically opening a more efficient energy relaxation channel.

ACKNOWLEDGMENTS

Our collaboration was supported in part by a Grant-in-Aid for Scientific Research from the Japan Society for the Promotion of Science (Grant No. 21540390). S.L. was also supported in part by the Croatian Ministry of Science, Education and Sport (Project No. 0982915-2899).

[1] Y. Fukumoto and S. Lugomer, Phys. Lett. A **308**, 375 (2003).
[2] S. Lugomer, Phys. Lett. A **361**, 87 (2007).
[3] S. Lugomer, Y. Fukumoto, B. Farkas, T. Szörényi, and A. Toth, Phys. Rev. E **76**, 016305 (2007).
[4] S. Lugomer and Y. Fukumoto, Fluid Dyn. Res. **36**, 277 (2005).
[5] L. E. Becker and M. J. Shelley, Phys. Rev. Lett. **87**, 198301 (2001).
[6] V. B. Eltsov, R. Blaauwgeers, N. B. Kopnin, M. Krusius, J. J. Ruohio, R. Schanen, and E. V. Thuneberg, Phys. Rev. Lett. **88**, 065301 (2002).
[7] B. A. Korgel, Science **303**, 1308 (2004).
[8] Z. L. Wang, X. Y. Kong, and Y. Ding, Microsc. Microanal. **10** (Suppl. 2), 528 (2004).
[9] Z. W. Pan, Z. R. Dai, and Z. L. Wang, Science **291**, 1947 (2001).
[10] Z. R. Dai, Z. W. Pan, and Z. L. Wang, Solid State Commun. **118**, 351 (2001).
[11] M. W. Murphy, P. S. G. Kim, X. Zhou, J. Zhou, M. Coulliard, G. A. Botton, and T. K. Shaw, J. Phys. Chem. C **113**, 4755 (2009).
[12] C. Borchers, D. Stichtenoth, S. Muller, D. Schwen, and C. Ronning, Nanotechnology **17**, 1067 (2006).
[13] S. McKernan, G. J. Zhu, and B. Carter, Philos. Mag. Lett. **64**, 349 (1991).
[14] T. Hanrath and B. A. Korgel, Adv. Mater. **15**, 437 (2003).
[15] L. Yang, X. Zhang, R. H. Zhang, and X. An, Solid State Commun. **130**, 769 (2004).
[16] K. C. Lo, H. P. Ho, K. Y. Fu, and P. K. Chu, Surf. Coat. Technol. **201**, 6804 (2007).
[17] Z.-Y. Yuan, J.-F. Colomwer, and B.-L. Su, Chem. Phys. Lett. **363**, 362 (2002).
[18] S. Tanda, T. Tsuneta, K. Yamaya, and N. Hatakanaka, Nature (London) **417**, 397 (2002).
[19] S. Biswas, S. Kar, T. Ghoshai, V. D. Ashok, S. Chakrabarti, and S. Chaudri, Mater. Res. Bull. **42**, 428 (2007).
[20] M.-F. Yu, M. J. Dyer, J. Chen, D. Qian, W. K. Liu, and R. S. Ruoff, Phys. Rev. B **64**, 241403 (2001).
[21] S. Motojima and X. Chen, Bull. Chem. Soc. Jpn. **80**, 449 (2007).
[22] R. Gao, Z. L. Wang, and S. Fan, J. Phys. Chem. B **104**, 1227 (2000).
[23] A. Szabo, A. Fonsca, J. B. Nagy, Ph. Lambin, and L. P. Biro, Carbon **43**, 1628 (2005).
[24] G. Bellesia, M. V. Fedorov, and E. G. Timoshenko, J. Chem. Phys. **128**, 195105 (2008).
[25] T. Strick, J.-F. Allemand, D. Bensimon, R. Lavery, and V. Croquette, Physica A **263**, 392 (1999).
[26] M. D. Frank-Kamenetskii, J. Mol. Struct.: THEOCHEM **336**, 235 (1995).
[27] S. Koombhongse, W. Liu, and D. H. Reneker, J. Polym. Sci., B, Polym. Phys. **39**, 2598 (2001).
[28] W. Xie, H. Zhang, and H. Wang, Sol. Phys. **254**, 271 (2008).
[29] C. Liu, J. Lee, D. E. Gary, and H. Wang, Astrophys. J. **658**, L127 (2007).
[30] H. K. Moffatt and R. L. Ricca, Proc. R. Soc. London, Ser. A **439**, 411 (1992).
[31] A. Y. K. Chui and H. K. Moffatt, Proc. R. Soc. London, Ser. A **451**, 609 (1995).
[32] R. L. Ricca, *VII European Meeting on Solar Physics, Catania, Italy, 1994*, edited by G. Belvedere, M. Rodonó, B. Schnieder, and G. M. Simmett (Catania Astrophysical Observatory, Cantania, Italy, 1994), p. 151.
[33] R. L. Ricca, Fluid Dyn. Res. **36**, 319 (2005).
[34] A. Boudaoud, P. Patricio, and M. Ben Amar, Phys. Rev. Lett. **83**, 3836 (1999).
[35] W. Helfrich and J. Prost, Phys. Rev. A **38**, 3065 (1988).
[36] R. Ghafouri and R. Bruinsma, Phys. Rev. Lett. **94**, 138101 (2005).
[37] S. Zhao, S. Zhang, Z. Yao, and L. Zhang, Phys. Rev. E **74**, 032801 (2006).
[38] R. Osserman, *A Survey of Minimal Surfaces* (Dover, New York, 1986).
[39] A. Fogden and S. T. Hyde, Eur. Phys. J. B **7**, 91 (1999).
[40] S. Console and A. Fino, Geometria Riemanniana delle Superfici, http://www.dm.unito.it/personalpages/console/Dispense/superfici.pdf
[41] R. L. B. Selinger, J. V. Selinger, A. P. Malanoski, and J. M. Schnur, Phys. Rev. Lett. **93**, 158103 (2004).
[42] R. D. Kamien and T. C. Lubensky, Phys. Rev. Lett. **82**, 2892 (1999).
[43] C. Branden and T. Tooze, *Introduction to Protein Structure* (Garland Publishing Inc., New York, 1991).
[44] H. Havlicek, http://www.geometrie.tuwien.ac.at/havlicek/ergaenz.html
[45] Ya. B. Zeldovich, A. A. Ruzmaikin, and D. D. Sokoloff, *The Almighty Chance* (World Scientific, Singapore, 1990), p. 215.
[46] D. Moldovan and L. Golubovic, Phys. Rev. Lett. **82**, 2884 (1999).
[47] J. A. Åström, J. Timonen, and M. Karttunen, Phys. Rev. Lett. **93**, 244301 (2004).
[48] F. Cattaneo, Astrophysical Dynamo Action, http://www.newton.ac.uk/prgrammes/MSI/seminars/101211251.ppt
[49] M. Mukerjee, Sci. Am. **272**, 24 (1995).